

# Active Prompt Learning with Vision-Language Model Priors

Hoyoung Kim<sup>1</sup>   Seokhee Jin<sup>1</sup>   Changhwan Sung<sup>2</sup>   Jaechang Kim<sup>1</sup>   Jungseul Ok<sup>1,2\*</sup>

Graduate School of AI, POSTECH<sup>1</sup>,   Dept. of CSE, POSTECH<sup>2</sup>  
 {hoyoung.kim, jin749, chseung, jaechang, jungseul}@postech.ac.kr

## Abstract

*Vision-language models (VLMs) have demonstrated remarkable zero-shot performance across various classification tasks. Nonetheless, their reliance on hand-crafted text prompts for each task hinders efficient adaptation to new tasks. While prompt learning offers a promising solution, most studies focus on maximizing the utilization of given few-shot labeled datasets, often overlooking the potential of careful data selection strategies, which enable higher accuracy with fewer labeled data. This motivates us to study a budget-efficient active prompt learning framework. Specifically, we introduce a class-guided clustering that leverages the pre-trained image and text encoders of VLMs, thereby enabling our cluster-balanced acquisition function from the initial round of active learning. Furthermore, considering the substantial class-wise variance in confidence exhibited by VLMs, we propose a budget-saving selective querying based on adaptive class-wise thresholds. Extensive experiments in active learning scenarios across nine datasets demonstrate that our method outperforms existing baselines.*

## 1. Introduction

Vision-language models (VLMs), such as CLIP [42] and ALIGN [24], have demonstrated impressive zero-shot capabilities across various downstream tasks, including object detection [10, 12, 57], semantic segmentation [14, 31, 54], and image classification [42, 46, 56], by aligning visual and textual information within a shared representation space [24, 42, 55]. Nevertheless, as VLMs rely on manually crafted text prompts for each task, which can be time-consuming and labor-intensive, efficiently adapting VLMs to new tasks remains crucial. Prompt learning has emerged as a promising solution, particularly for image classification tasks, allowing VLMs to learn task-specific prompts without the computational burden of directly fine-tuning image

and text encoders.

Generally, prompt learning methods have focused on model-centric approaches, modifying prompt architectures and learning objectives. Specifically, researchers have introduced various types of prompts, including text prompts [59], image-conditioned text prompts [58] for text encoders, and multimodal prompts that work across both image and text encoders [25]. In terms of learning objectives, prompts are initially trained with cross-entropy loss [59], supplemented by regularization terms to maintain CLIP’s general knowledge [60] and incorporate task-agnostic knowledge [40], which helps prevent overfitting on specific tasks. However, these model-centric methods prioritize leveraging VLM priors to optimize prompts with given few-shot labeled datasets, often overlooking the budget-efficient potential of data selection, which can achieve higher accuracy with fewer labeled data.

Unlike previous methods focused on fully utilizing VLM priors for prompt learning, we leverage them to select informative data. In this context, active learning offers an alternative by prioritizing the labeling of the most informative images with minimal budgets. Recently, active prompt learning has been proposed [4], revealing that class-balanced data selection is key to mitigate the imbalanced knowledge of VLMs. However, this approach merely adheres to the conventional few-shot datasets, disregarding rather than leveraging VLMs. To address this, we propose an efficient active prompt learning for VLMs, which incorporates a class-guided clustering and a selective querying.

For a class-guided clustering, we leverage the pre-trained image and text encoder of VLMs. In detail, we first derive class-guided features by averaging two components: (i) image features from the image encoder and (ii) text features computed as a weighted sum of each class’s text features, with weights based on similarity scores to the image features. We then apply  $K$ -means clustering [34] on these class-guided features to achieve balanced data selection across clusters. While traditional active learning often encounters the cold-start problem due to a lack of reliable methods to evaluate data in the initial round [7, 35], our

\*Corresponding author.

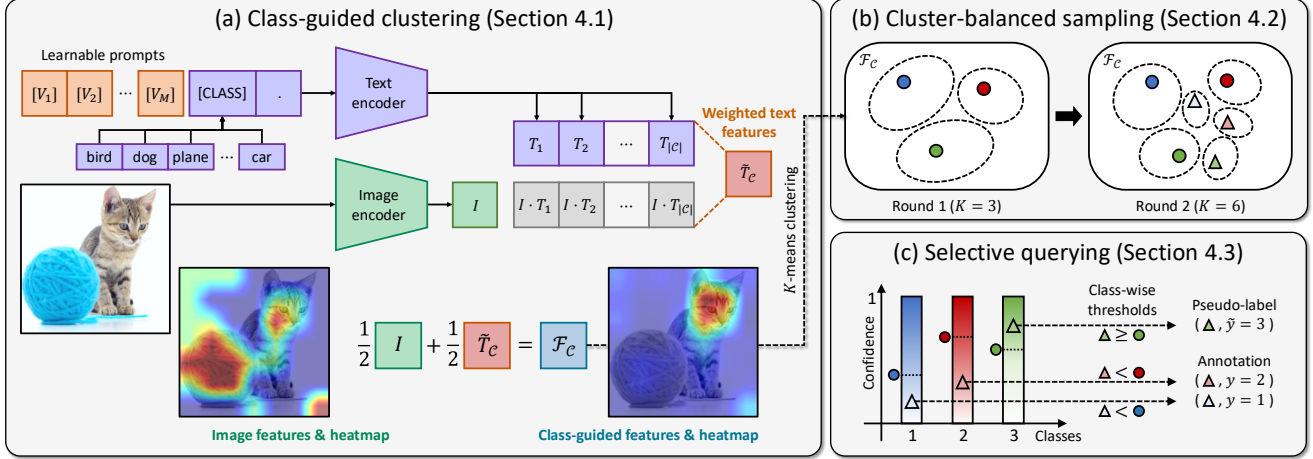


Figure 1. *An overview of the proposed framework.* (a) Class-guided features  $\mathcal{F}_C$  are obtained by averaging the image features  $I$  with the weighted text features  $\tilde{T}_C$ , using similarity scores as weights. In the heatmaps,  $\mathcal{F}_C$  focus on the guided-classes  $C = \{\text{Cat}, \text{Dog}\}$  than  $I$ . (b)  $K$ -means clustering is performed on  $\mathcal{F}_C$ . With an increasing  $K$ , cluster-balanced sampling becomes available in each round. (c) The confidence scores of previously labeled data (circles) serve as thresholds for new candidates (triangles). If a candidate’s confidence exceeds its corresponding threshold, a pseudo-label is assigned to conserve the budget, otherwise it is labeled by annotators.

cluster-balanced acquisition function provide the benefit of a warm-start. However, diversity-focused acquisitions may inefficiently allocate budget to data in which VLMs are already confident.

To address this issue, we introduce a budget-saving selective querying based on adaptive class-wise thresholds. Since VLMs often exhibit substantial variance in confidence across different downstream tasks and even among individual classes [4], we implement adaptive class-wise thresholds without adding extra hyperparameters. Specifically, we assign pseudo-labels to the data selected by the class-balanced acquisition when their confidence scores exceed the relevant threshold. Consequently, we can conserve budget in each round rather than exhausting it entirely.

The proposed framework, illustrated in Figure 1, fully leverages VLM priors to enable efficient adaptation across various classification tasks. Beyond simply employing the two encoders of CLIP [42] for clustering [33], we further analyze the advantages of incorporating the weighted text features through visualization tools, such as GradCAM [44] in Figure 2 and T-SNE [49] in Figure 4. Extensive experiments in active learning scenarios demonstrate that our cluster-balanced acquisition with selective querying outperforms other baselines.

Our main contributions are summarized as follows:

- We propose a budget-efficient active prompt learning for VLMs, particularly on CLIP, where the class-guided clustering and the selective querying fully leverage VLM priors (Sections 4.1 and 4.3).
- We provide in-depth analyses of the class-guided features and clustering with GradFAM, a variant of GradCAM,

and T-SNE, respectively (Figures 2 and 4).

- Experiments demonstrate that our method achieve superior budget efficiency and performance across diverse active learning scenarios (Sections 5.2).
- We explore the potential for extending of our data-centric approach into existing model-centric prompt learning methods (Section 5.3).

## 2. Related Work

**Prompt Learning in Vision-Language Models.** To address the inefficiency of fine-tuning all VLM parameters, CoOp [59] proposes prompt learning focused on compact prompts for efficient adaptation. Subsequent works [25, 26, 32, 40, 58] have further developed CoOp, adopting model-centric approaches such as modifying prompt architectures [25] and learning objectives [60]. For instance, MaPle [25] incorporates multi-modal prompts that jointly consider both VLM encoders, while ProGrad [60] introduces an auxiliary loss term to maintain general knowledge of CLIP. In contrast, PCB [4] efficiently adapts VLMs from a data-centric perspective by employing an active learning with a pseudo class-balanced acquisition function. While PCB’s acquisition focuses on mitigating the imbalanced prior knowledge of VLMs, we fully exploit VLM priors across the proposed method.

**Active Learning in the Era of Foundation Models.** We are in an era where foundation models, such as CLIP [42], SAM [29], and GPT-4 [38], dominate a wide range of downstream tasks. Their impressive generalization capabilities may imply that the role of active learning is becoming less

significant. However, recent studies continue to actively leverage the prior knowledge embedded in foundation models [5, 15, 28, 50] to further enhance budget efficiency with active learning. For instance, ALC [28] introduces correction queries to refine SAM-generated labels in semantic segmentation tasks, while ActiveLLM [5] addresses the cold start problem by utilizing LLMs in text classification tasks. Here, we fully leverage VLM priors to enhance performance in image classification tasks.

**Acquisition Functions in Active Learning.** Active learning employs various acquisition functions to identify the most informative samples for annotation, aiming to maximize model performance within a constrained budget. These acquisitions are broadly categorized into those focused on uncertainty [1, 13, 19, 39], diversity [45, 47, 53], and both [2, 22, 23, 27, 51]. Recent studies show that uncertainty-based acquisitions are more effective with higher budgets, while diversity-based ones perform better with lower budgets [16–18]. Building on this, we propose a cluster-balanced acquisition to adapt VLMs within limited budgets. In addition, we introduce a selective querying with adaptive class-wise thresholds to further conserve budget.

### 3. Preliminaries

For efficient adaptation in vision-language models (VLMs), we fully leverage their prior knowledge. Before presenting our method, we first outline the structure of VLMs and the relevant priors, in Section 3.1, which are utilized in our method. After that, we describe the basics of prompt learning with few-shot datasets in Section 3.2.

#### 3.1. VLM Priors

Pre-trained VLMs have shown decent zero-shot performance across various classification tasks. Specifically, the CLIP model  $\theta$  [42] comprises an image encoder  $\theta_{\text{img}}$  and a text encoder  $\theta_{\text{txt}}$ , performing zero-shot inference on an image  $x$  for a target class  $c \in \mathcal{C}$  using cosine similarity as:

$$p_{\theta}(y=c|x;t,\mathcal{C}) := \frac{\exp(\cos(\theta_{\text{img}}(x), \theta_{\text{txt}}(t_c))/\tau)}{\sum_{k \in \mathcal{C}} \exp(\cos(\theta_{\text{img}}(x), \theta_{\text{txt}}(t_k))/\tau)}, \quad (1)$$

where the text prompt  $t$  can be set as “a photo of a”, and  $t_c$  represents the concatenation of  $t$  and “[CLASS].” with the class token replaced by the class name  $c$ . Here,  $\tau$  denotes a temperature parameter. Considering the highest probability among all classes, we can obtain the pseudo label of an image  $x$  as follows:

$$y_{\theta}(x;t,\mathcal{C}) := \arg \max_{c \in \mathcal{C}} p_{\theta}(y=c|x;t,\mathcal{C}). \quad (2)$$

We note that the pseudo label depends on the text prompt  $t$  and the target class set  $\mathcal{C}$ . In Section 4, we leverage the pre-trained image and text encoders of CLIP for our

---

#### Algorithm 1 Proposed Active Prompt Learning

---

**Require:** Image set  $\mathcal{I}$ , learnable prompts  $t$ , budget per round  $B$ , and final round  $R$

- 1: **for**  $r = 1, 2, \dots, R$  **do**
  - 2:   Obtain class-guided features  $\forall i \in \mathcal{I}$  via (7)
  - 3:   K-means clustering on the class-guided features
  - 4:   Select cluster-balanced candidate images via (9)
  - 5:   Compute adaptive class-wise thresholds via (11)
  - 6:   Build dataset  $\mathcal{D}_r$  with a selective querying as (12)
  - 7:   Obtain prompts  $t_r$  training with  $\mathcal{D}_r$  via (13)
  - 8: **end for**
  - 9: **return** Final dataset  $\mathcal{D}_R$  and prompts  $t_R$
- 

class-guided clustering and the pseudo label for our selective querying.

#### 3.2. Prompt Learning in VLMs

Vision-language models (VLMs) contain numerous parameters, which makes fine-tuning on a small labeled dataset impractical. Recently, prompt learning has facilitated efficient adaptation in VLMs by freezing the image and text encoders and focusing on learning input prompts. For instance, CoOp [59] introduces learnable vectors into the text prompt  $t_c$  of class  $c$ , replacing the conventional “a photo of a [CLASS].” text prompts with:

$$t_c = [V_1][V_2] \dots [V_M][\text{CLASS}]., \quad (3)$$

where each  $V$  represents a learnable vector and  $M$  denotes the number of vectors. These vectors in  $t$  are trained on a dataset  $\mathcal{D}$  by minimizing the cross-entropy (CE) loss:

$$\hat{\mathbb{E}}_{(x,y) \sim \mathcal{D}} [\text{CE}(y, p_{\theta}(y; x, t, \mathcal{C}))]. \quad (4)$$

In this context, previous prompt learning methods have primarily taken a model-centric perspective, aiming to maximize model performance on the given training dataset  $\mathcal{D}$ . From a data-centric perspective, however, building datasets requires human labor, making active learning essential for creating information-dense datasets while minimizing interactions with annotators. In addition, we note that our data-centric approach is compatible with existing model-centric prompt learning methods.

### 4. Proposed Active Prompt Learning

Given an unlabeled image set  $\mathcal{U}$ , we consider a general active learning scenario for image classification tasks, where annotators are asked to label each image  $x \in \mathcal{U}$  with its accurate label  $y \in \mathcal{C} := \{1, 2, \dots, C\}$ . For each round  $r$ , with a maximum budget of  $B$ , we begin by constructing a candidate set of  $B$  images from  $\mathcal{U}_r$  utilizing class-guided clustering. Each candidate is then evaluated with a class-wise

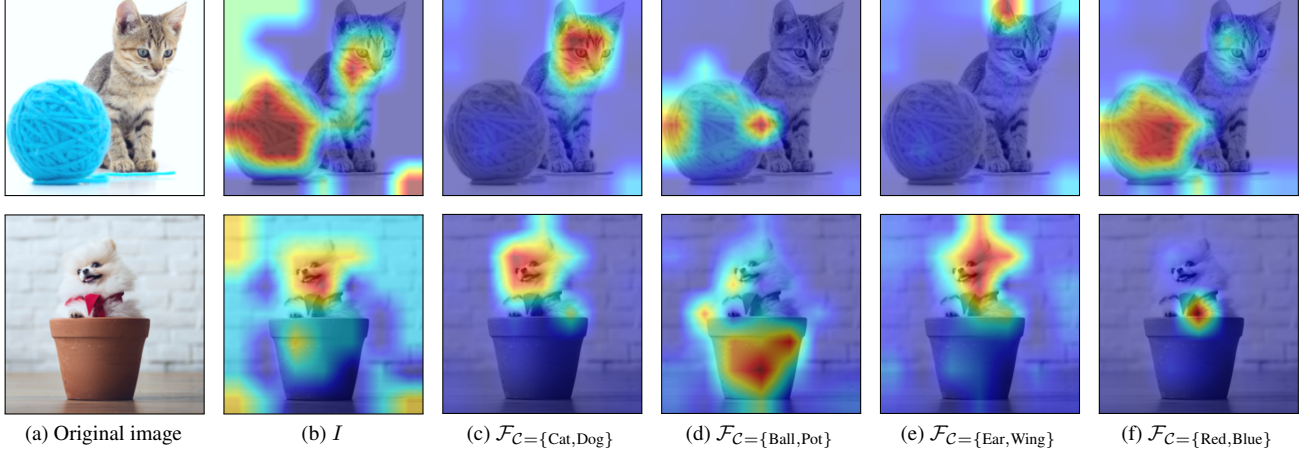


Figure 2. *GradFAM with various target features.* (b) All objects in the image significantly impacts the target image features  $I$ . (c-f) With our class-guided features  $\mathcal{F}_C$  for target features, the heatmap aligns with the target classes  $\mathcal{C}$ . Further details are in the Appendix A.

threshold to determine whether to acquire ground-truth labels from annotators or use pseudo labels to conserve budget. Finally, learnable prompts  $t_r$  are trained by prompt learning on the dataset  $\mathcal{D}_r$  accumulated up to round  $r$ .

In the followings, we introduce a class-guided clustering, which leverages the pre-trained image and text encoders of CLIP (Section 4.1), and a cluster-balanced acquisition function to select candidate images (Section 4.2). After that, we introduce a budget-saving selective querying (Section 4.3). The overall algorithm is described in Algorithm 1.

#### 4.1. Class-Guided Clustering

Conventional active learning often relies on random sampling to construct the initial dataset, which can lead to the cold-start problem. In contrast, we fully utilize CLIP’s pre-trained image and text encoders for class-guided clustering, which can be applied at each round of the active learning process. To construct class-guided features of an image  $x$ , we first define its image and text features,  $I(x)$  and  $\tilde{T}_C(x)$ , respectively. For the image features, we simply use the image encoder of CLIP as follows:

$$I(x) := \theta_{\text{img}}(x). \quad (5)$$

To derive the text features of  $x$ , we compute a weighted combination of text features with soft labels as weights:

$$\tilde{T}_C(x; t_{r-1}) := \sum_{c \in \mathcal{C}} p_{\theta}(y = c \mid x, t_{r-1}) \theta_{\text{txt}}(t_{r-1, c}), \quad (6)$$

where  $t_{r-1}$  represents the learned vectors from the previous round, and  $t_{r-1, c}$  concatenates  $t_{r-1}$  with class  $c$  as described in (3). For the initial round, we set  $t_{r-1}$  as “a photo of a ”. Finally, we average the image and text features to obtain the class-guided features  $\mathcal{F}_C(x)$  for image  $x$  as:

$$\mathcal{F}_C(x; t_{r-1}) := \frac{I(x) + \tilde{T}_C(x; t_{r-1})}{2}. \quad (7)$$

After that, we apply the  $K$ -means clustering algorithm [34] on the set of class-guided features across all images to partition them into  $K$  clusters.

**GradFAM on Class-Guided Features.** We modify GradCAM [44] into GradFAM (Gradient-weighted Feature Activation Mapping) to visualize the influence of class-guided features on an image. GradCAM highlights the degree to which individual pixels contribute to a specific class by analyzing the gradients of the class score with respect to the feature maps. To tailor GradCAM for VLMs, we introduce the concept of *target features* denoted by  $\mathcal{F}_{\text{target}}$ , allowing GradCAM to visualize the influence of target features on an image  $x$  based on the cosine similarity score defined as  $\cos(I(x), \mathcal{F}_{\text{target}})$ . Our analysis technique, called GradFAM, visualizes the influence of target features rather than target class, offering the advantage of enabling label-free analysis. Figure 2b represents the case where  $\mathcal{F}_{\text{target}} = I(x)$ . Consistent with CLIP’s approach of embedding images and texts into a shared space, we observe that the influence of the target image features primarily concentrates on the overall objects within the image. On the other hand, when the target features are guided by the set of classes, *i.e.*  $\mathcal{F}_{\text{target}} = \mathcal{F}_C(x; t)$  where  $t$  is “a photo of a ”, Figures 2c to 2f distinctly highlight the specific objects corresponding to the guiding class sets. We note that our class-guided features incorporates class-relevant information through the text encoder, potentially resulting in clustering that aligns more closely with the target classifier, as described in Figure 4.

#### 4.2. Cluster-Balanced Acquisition Function

For ease of explanation, we first outline the data selection process in the initial round of active learning. For a cluster-balanced acquisition, we set the number of clusters  $K$  equal to the budget  $B$ , allowing for the selection of one image per



cluster. To choose the most representative sample from each cluster  $C_i$ , we first calculate its centroid  $c_i$  as follows:

$$c_i := \frac{1}{|C_i|} \sum_{x \in C_i} \mathcal{F}_C(x; t). \quad (8)$$

The closest image  $x_i^*$  to the centroid  $c_i$  is then selected as:

$$x_i^* = \arg \min_{x \in C_i} \|\mathcal{F}_C(x; t) - c_i\|_2. \quad (9)$$

We can construct the set of candidate images for querying:

$$\mathcal{Q} := \{x_1^*, x_2^*, \dots, x_B^*\}. \quad (10)$$

In the initial round, we consume the entire budget  $B$  to request annotations for all candidate images in  $\mathcal{Q}$ . Here,  $t$  is replaced by  $t_{r-1}$ , and  $\mathcal{Q}$  by  $\mathcal{Q}_r$  for a subsequent round  $r$ .

**Subsequent rounds with increasing  $K$ .** To enhance the diversity in the selected data, we introduce a progressively increasing  $K$  based on round  $r$ , *i.e.*  $K = B \times r$ . This linear increase in  $K$  ensures that at least  $B$  clusters remain unlabeled in each round, allowing for the selection of clusters not included in previous rounds. However, due to the inaccuracy of clustering in earlier rounds, samples previously assigned to different clusters may now be classified into the same cluster. To address these instances, we prioritize the larger clusters among all unlabeled clusters.

### 4.3. Selective Querying

In each round  $r$ , we can allocate the entire budget  $B$  to acquire labels for all candidate images in  $\mathcal{Q}_r$ . However, CLIP has demonstrated decent zero-shot performance in downstream classification tasks [42] and performs even better with a few labeled samples [59]. Therefore, for a candidate image where CLIP is already sufficiently confident in its label, we skip manual labeling and apply a pseudo label to conserve budget.

Since CLIP’s knowledge is imbalanced across classes in classification tasks [4], we propose a selective querying with class-wise thresholds that operate without hyperparameters. To this end, we leverage the confidence scores of images from the previous training dataset  $\mathcal{D}_{r-1}$ . In round  $r$ , the threshold  $\epsilon_{r,c}$  for class  $c \in \mathcal{C}$  is computed as:

$$\epsilon_{r,c} := \frac{1}{|\mathcal{D}_{r-1,c}|} \sum_{(x,y=c) \in \mathcal{D}_{r-1,c}} p_\theta(y | x; t_{r-1}, \mathcal{C}), \quad (11)$$

where  $\mathcal{D}_{r-1,c}$  represents the subset of the training dataset labeled as  $c$ . Note that thresholds for round  $r$  depend on prior information, including  $\mathcal{D}_{r-1}$  and  $t_{r-1}$ . Therefore, a selective querying is impossible in the initial round. We finally apply pseudo labels to candidates if their confidence exceeds the corresponding threshold. As a result, the

dataset  $\mathcal{D}_r$  at round  $r$  can be constructed as follows:

$$\mathcal{D}_r := \{(x, y) \mid x \in \mathcal{Q}_r, p_\theta(\tilde{y} | x; t_{r-1}, \mathcal{C}) < \epsilon_{r,\tilde{y}}\} \cup \mathcal{D}_{r-1} \cup \{(x, \tilde{y}) \mid x \in \mathcal{Q}_r, p_\theta(\tilde{y} | x; t_{r-1}, \mathcal{C}) \geq \epsilon_{r,\tilde{y}}\}, \quad (12)$$

where the pseudo label  $\tilde{y} = y_\theta(x; t, \mathcal{C})$  is defined as in (2). Here, we note that  $|\mathcal{D}_r| = B \times r$ , yet the budget required is actually lower thanks to our selective querying.

To avoid bias in prompts trained during the previous round, we reinitialized  $t_r$  randomly at each round and train prompts by minimizing the following CE loss:

$$\hat{\mathbb{E}}_{(x,y) \sim \mathcal{D}_r} [\text{CE}(y, p_\theta(y; x, t_r, \mathcal{C}))]. \quad (13)$$

## 5. Experiments

### 5.1. Experimental Setup

**Datasets & Implementation Details.** Following previous studies [4, 42, 59], we use nine publicly available image classification datasets: Food101 (food images) [6], OxfordPets (various pet species) [41], FGVC Aircraft (aircraft types) [36], Caltech101 (general object categories) [11], SUN397 (scene recognition) [52], Flowers102 (flower species) [37], DTD (texture patterns) [8], Stanford-Cars (car models) [30], and UCF101 (human actions) [48]. In our experiments, we employ CLIP ViT-B/32 [9, 42] as our VLM. More details are in the Appendix B

### 5.2. Active Learning Scenario

**Baselines.** Our cluster-balanced acquisition with selective querying (CB+SQ) is compared with the state-of-the-art (SOTA) active prompt learning method for VLMs, known as pseudo-class balance (PCB) [4], which operates based on BADGE [3]. In addition, we compare with conventional acquisitions commonly used in active learning for classification tasks, including Random, Entropy [21] and Core-Set [45]. To facilitate a focused comparison of acquisition functions, all training is conducted using CoOp [59], with LLM descriptions excluded from all baselines.

**Evaluation Protocol.** For a fair comparison, we follow the existing active learning scenario in PCB [4]. Specifically, experiments are conducted over 8 rounds, with the maximum budget per round set to the number of classes, *i.e.*  $B = |\mathcal{C}|$ . Since the total budget varies across datasets, we assume 100% budget usage by the 8th round, with the maximum allocation of 12.5% per round. Here, a budget of one indicates that an oracle assigns the ground-truth label for a single image. Thanks to our selective querying in CB+SQ, we generally consume less than 12.5% of the total budget per round from the second round onward. We report the average accuracy over three trials, with shaded regions in the graphs representing the standard deviation.

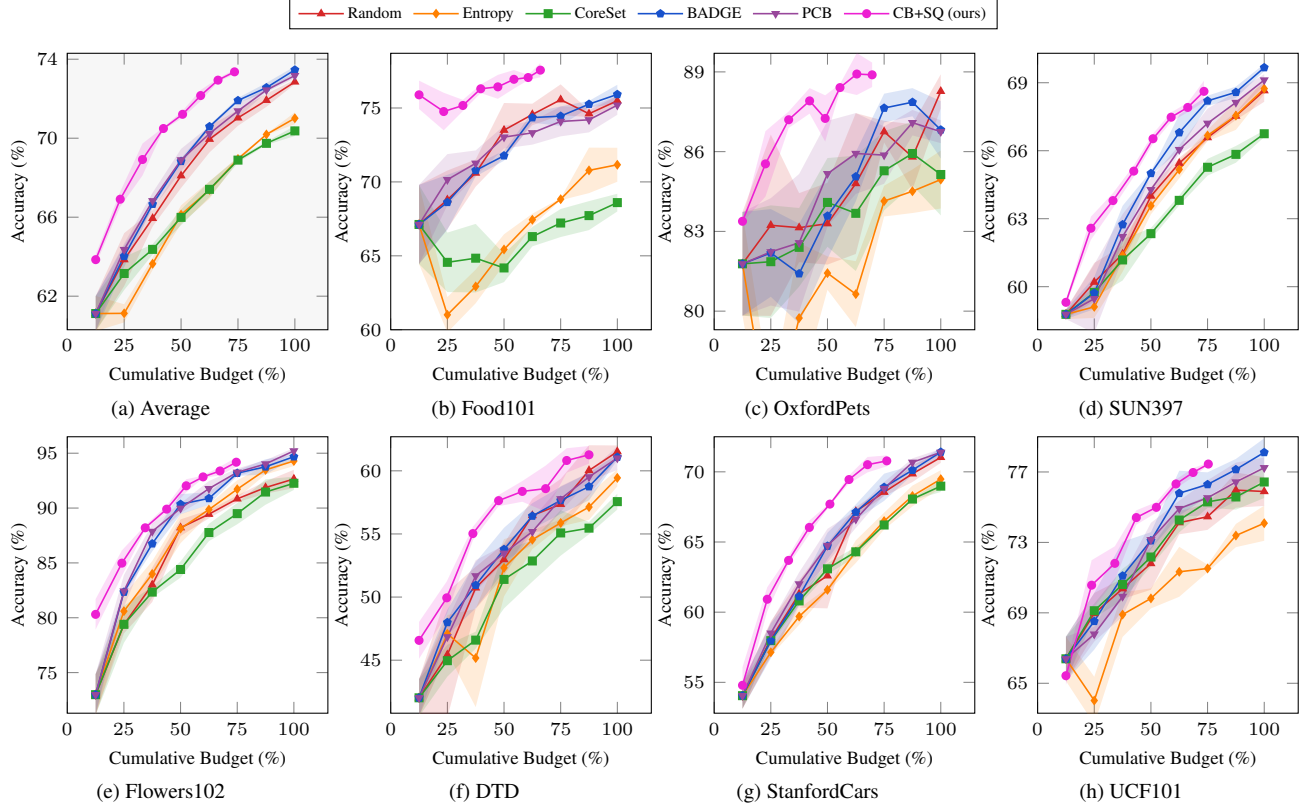


Figure 3. *Effect of the proposed acquisition.* (a) Our CB+SQ outperforms the other baselines in average performance across 9 datasets. (b-h) We achieve comparable performance to other baselines, while reducing the cumulative budget by 12% to 41% across all datasets.

Methods	Food101	OxfordPets	Aircraft	Caltech101	SUN397	Flowers102	DTD	StanfordCars	UCF101	Average (%)
MaPle	72.37	85.27	18.33	91.57	61.43	75.23	48.77	57.30	69.33	64.40
+ CB	77.63	86.47	18.23	91.50	62.27	<b>80.97</b>	48.67	57.53	67.53	65.64
+ CB*	<b>78.67</b>	<b>86.57</b>	<b>18.40</b>	<b>91.73</b>	<b>64.10</b>	78.27	<b>51.07</b>	<b>60.27</b>	<b>71.27</b>	<b>66.70</b>
PromptSRC	78.47	<b>89.60</b>	18.67	93.10	66.80	77.60	52.37	63.67	72.90	68.13
+ CB	80.53	88.10	21.03	92.23	66.17	<b>80.30</b>	52.03	61.50	71.00	68.10
+ CB*	<b>81.03</b>	89.07	<b>24.20</b>	<b>93.47</b>	<b>68.67</b>	78.63	<b>54.07</b>	<b>63.77</b>	<b>74.13</b>	<b>69.67</b>
ProMetaR	77.07	87.63	19.50	92.53	64.93	78.87	52.07	60.60	72.57	67.31
+ CB	80.03	87.33	20.27	91.93	65.00	<b>81.90</b>	52.33	59.03	70.83	67.63
+ CB*	<b>80.30</b>	<b>88.67</b>	<b>21.70</b>	<b>93.40</b>	<b>68.03</b>	80.60	<b>55.27</b>	<b>62.53</b>	<b>74.17</b>	<b>69.41</b>

Table 1. *Synergy of the proposed acquisition with existing prompt learning methods.* All baseline methods are trained with 1-shot datasets. Our CB\*-based curated datasets enhance the performance of previous model-centric prompt learning methods.

**Effect of Various Acquisitions.** Figure 3 demonstrates the effectiveness of our proposed acquisition CB+SQ. While other baselines suffer from a cold-start problem due to Random acquisition in the initial round, our CB+SQ leverages the pre-trained image and text encoders of CLIP to enable a warm-start, resulting in an average performance increase of 2.7% as depicted in Figure 3a. This performance difference remains consistent across all eight rounds. In addition, our selective querying allows CB+SQ to achieve performance on par with other baselines while reducing the labeling bud-

get by 26%. We also observe the same phenomenon reported in [4], where existing acquisition methods, including Entropy and CoreSet, perform worse than Random. We further analyze this result in Section 5.3.

### 5.3. Further Analyses

**Extensions to SOTA Model-Centric Prompt Learning Methods.** Our cluster-balanced (CB) acquisition effectively selects informative images by utilizing a pre-trained CLIP model. These selected images can be directly applied to enhance the performance of SOTA model-centric

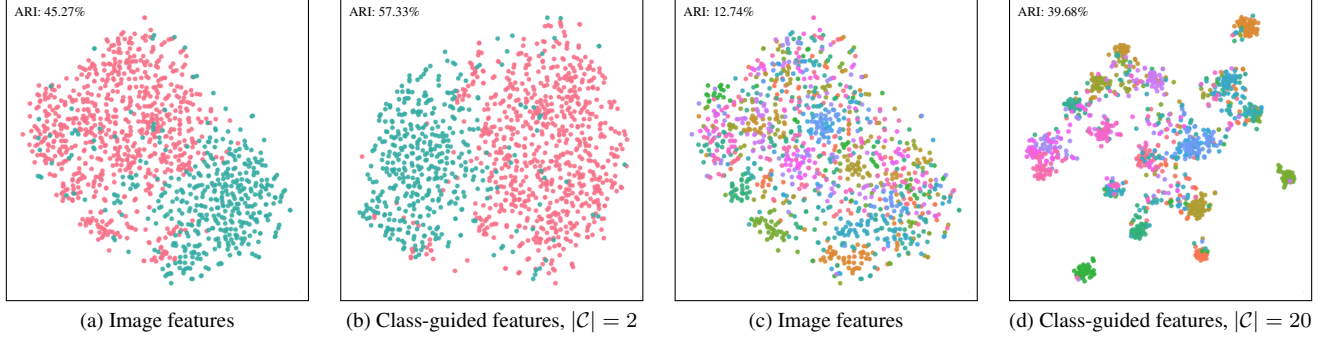


Figure 4. *T-SNE for class-guided clustering.* (a, c) Clustering based solely on image features results in clusters that are poorly separated. (b, d) In contrast, our class-guided clustering, which incorporates class information, leads to more distinct clusters that align with the size of the guiding class set  $C$ .

Image Features	Text Features	Labels	Average Acc. (%)
✓	✗	✗	61.19 $\pm$ 0.53
✗	✓ <sub>soft</sub>	✗	59.41 $\pm$ 1.02
✓	✓ <sub>soft</sub>	✗	<b>63.82</b> $\pm$ 0.90
✗	✗	✓	61.01 $\pm$ 1.84
✓	✓ <sub>label</sub>	✓	<b>66.87</b> $\pm$ 0.52

Table 2. *Ablation on different feature spaces.* In the initial round, our class-guided features in the third row, which incorporate both image and text features, demonstrate effectiveness across 9 datasets.

Image Features	Text Features	Labels	EuroSAT Acc. (%)
✓	✗	✗	<b>58.92</b> $\pm$ 2.25
✓	✓ <sub>hard</sub>	✗	39.58 $\pm$ 1.98
✓	✓ <sub>soft</sub>	✗	53.32 $\pm$ 0.86
✗	✗	✓	52.20 $\pm$ 1.92
✓	✓ <sub>label</sub>	✓	<b>65.30</b> $\pm$ 1.75

Table 3. *Negative effect of text features.* In the EuroSAT dataset, the image features are the most effective choice for our cluster-balanced acquisition. Here, ✓<sub>hard</sub> and ✓<sub>soft</sub> differ in the type of weights used, based on hard and soft pseudo labels, respectively.

prompt learning methods, including MaPle [25], PromptSRC [26], and ProMetaR [40]. Table 1 represents that our CB-based datasets slightly outperforms the conventional 1-shot datasets, which contain one labeled image per class. However, the 1-shot datasets differ from active learning, which start with unlabeled images. For a fair comparison with them, we construct CB\*-based datasets, where the weighted text features in (6) are replaced with the text features of the ground-truth label. In Table 1, our CB\*-based datasets outperform other baselines, emphasizing the importance of data-centric approaches for efficient adaptation in VLMs. More experiments are in the Appendix B.

**Visualization for Class-Guided Clustering.** In Section 4.1, we analyze the proposed class-guided features using GradFAM, as shown in Figure 2. Here, we further visualize the impact of class-guided features on clustering with T-SNE [49] on the Waterbirds dataset [43]. Specifically, the Waterbirds dataset consists of 200 distinct bird species, where each image is labeled by habitat (water, land), background (water, land), and specific species. This allows us to categorize the dataset into 2, 4, or 200 groups. For improved visual clarity, we analyze a subsample of 20 classes. Figures 4a and 4c shows that the limitation of relying solely on

image features in capturing semantic information. In contrast, our class-guided features, which incorporate the set of classes  $C$ , effectively reflect relevant class information in the clustering results, as illustrated in Figures 4b and 4d. More details are in the Appendix C.

**Effect of Various Feature Spaces.** In Table 2, we examine the effect of various feature spaces on our cluster-balanced acquisition, as an alternative to the proposed class-guided features that leverage both Image and Text features. Table 2 demonstrates that our class-guided features yield a 2.6% and 4.4% improvement over using only Image or only Text features, respectively. In addition, we experiment with a conventional few-shot labeled dataset that relies solely on Labels for a perfectly class-balanced dataset, which can be impractical in an active learning scenario. For a fair comparison, we redefine the weighted text features in (6) as the text features of ground-truth labels, resulting in an average performance increase of 5.8%.

**Limitation of Class-Guided Clustering.** Our class-guided features leverage the pre-trained image and text encoders of CLIP. While these features are effective across various datasets, as shown in Table 2, we find that using only image

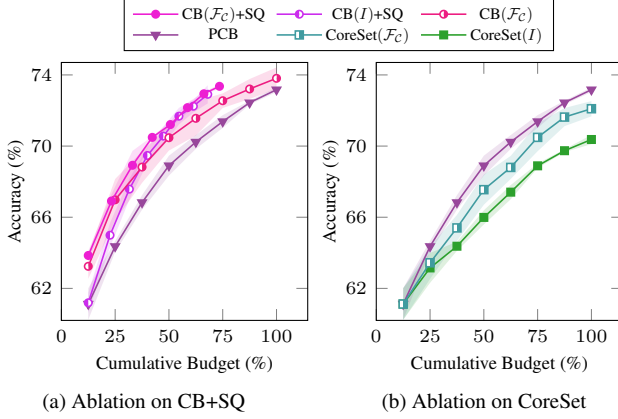


Figure 5. *Ablation with proposed components.* (a) Even with a single component removed, our method still outperforms PCB. (b) The performance of CoreSet improves with the incorporation of our class-guided features.

Methods	Base	Novel	HM
Random	59.02 $\pm$ 1.06	58.94 $\pm$ 1.48	58.98 $\pm$ 1.14
CB	<b>68.81</b> $\pm$ 1.07	<b>63.68</b> $\pm$ 1.25	<b>66.15</b> $\pm$ 0.67

Table 4. *Effect of the proposed acquisition.* Our CB outperforms the other baselines across 9 datasets in the initial round.

features is more beneficial for the EuroSAT dataset [20], as demonstrated in Table 3. Originally, we obtain the weights for the weighted text features in (6) as soft pseudo-labels. However, converting these soft pseudo-labels to hard pseudo-labels results in a substantial drop in performance. Our findings suggest that entirely incorrect class guidance can impede performance. Nevertheless, since the text features with ground-truth labels yield a significant performance boost, the impact of text features can still be beneficial as VLMs continue to improve.

**Contribution of Each Proposed Component.** In Figure 5a, we analyze the influence of each proposed component in our cluster-balanced acquisition with selective querying (CB( $\mathcal{F}_C$ )+SQ): (i) class-guided features  $\mathcal{F}_C$ , and (ii) selective querying SQ. Each component is either replaced with image features  $I$  or removed, respectively. Figure 5a clearly illustrates the contribution of each component, demonstrating that our method surpasses the previous SOTA called PCB, even without one of our component. In addition, although CoreSet has demonstrated low performance in active learning for VLMs [4], this is primarily due to its reliance on image features alone. We observe that incorporating our class-guided features can enhance its performance to some extent, as shown in Figure 5b, though it still fails to surpass PCB. We note that active learning for conventional neural networks with image-only encoders

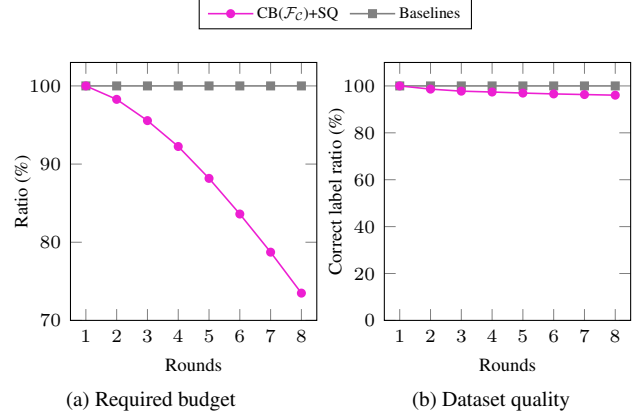


Figure 6. *Analyses of constructed datasets.* (a) As rounds progress, we construct datasets with progressively smaller budgets. (b) The quality of the constructed dataset remains consistently high, regardless of the number of rounds.

may differ from active learning for VLMs.

**Base-to-Novel Generalization.** Following previous work [59], we divide each dataset’s classes into base and novel groups. We then use acquisition functions to select a subset of unlabeled images from the base classes to train prompts, which are subsequently applied to the novel classes for evaluation. In Table 4, we compare our cluster-balanced (CB) acquisition with Random reflecting the cold-start of other acquisitions in Figure 3. Table 4 demonstrates that our CB acquisition outperforms Random in both base and novel groups. Here, HM denotes the harmonic mean of base and novel performance. Additional experiments are included in the Appendix B.

**Analyses of Constructed Datasets.** A primary goal of active learning is to construct high-quality datasets with minimal labeling budgets. Figure 6 demonstrates that our method builds high-quality datasets with a significantly smaller budget compared to previous methods. Specifically, while previous methods consume the entire budget each round to generate a 100% clean dataset, our selective querying conserves budget by using pseudo-labels based on class-wise thresholds, yet still achieves a comparable level of dataset quality. This results in performance on par with previous methods, as shown in Figure 3. Additionally, we note that as rounds progress, the budget-saving advantage of our method becomes even more pronounced.

## 6. Conclusion

In this work, we propose an efficient active prompt learning framework that leverages vision-language model priors. By utilizing the pre-trained image and text encoders of CLIP, we introduce the class-guided features, followed by  $K$ -means clustering on these features for our cluster-



balanced acquisition function. In addition, our selective querying with adaptive class-wise thresholds, results in improved budget efficiency. Extensive experiments demonstrate that our method outperforms baselines in active learning scenarios and further enhances the performance of previous model-centric prompt learning methods.

## References

- [1] Nabiha Asghar, Pascal Poupart, Xin Jiang, and Hang Li. Deep active learning for dialogue generation. In *Proceedings of the 6th Joint Conference on Lexical and Computational Semantics (\*SEM)*, 2017. 3
- [2] Jordan T Ash, Chicheng Zhang, Akshay Krishnamurthy, John Langford, and Alekh Agarwal. Deep batch active learning by diverse, uncertain gradient lower bounds. In *ICLR*, 2020. 3
- [3] Jordan T. Ash, Chicheng Zhang, Akshay Krishnamurthy, John Langford, and Alekh Agarwal. Deep batch active learning by diverse, uncertain gradient lower bounds. In *International Conference on Learning Representations*, 2020. 5
- [4] Jihwan Bang, Sumyeong Ahn, and Jae-Gil Lee. Active prompt learning in vision language models. In *Proceedings of the IEEE/CVF Conference on Computer Vision and Pattern Recognition*, pages 27004–27014, 2024. 1, 2, 5, 6, 8, 7
- [5] Markus Bayer and Christian Reuter. Activellm: Large language model-based active learning for textual few-shot scenarios. *arXiv preprint arXiv:2405.10808*, 2024. 3
- [6] Lukas Bossard, Matthieu Guillaumin, and Luc Van Gool. Food-101—mining discriminative components with random forests. In *Computer vision—ECCV 2014: 13th European conference, zurich, Switzerland, September 6–12, 2014, proceedings, part VI 13*, pages 446–461. Springer, 2014. 5
- [7] Liangyu Chen, Yutong Bai, Siyu Huang, Yongyi Lu, Bihan Wen, Alan Yuille, and Zongwei Zhou. Making your first choice: to address cold start problem in medical active learning. *Proceedings of Machine Learning Research—nnn*, 1:30, 2023. 1
- [8] Mircea Cimpoi, Subhransu Maji, Iasonas Kokkinos, Sammy Mohamed, and Andrea Vedaldi. Describing textures in the wild. In *Proceedings of the IEEE conference on computer vision and pattern recognition*, pages 3606–3613, 2014. 5
- [9] Alexey Dosovitskiy, Lucas Beyer, Alexander Kolesnikov, Dirk Weissenborn, Xiaohua Zhai, Thomas Unterthiner, Mostafa Dehghani, Matthias Minderer, Georg Heigold, Sylvain Gelly, Jakob Uszkoreit, and Neil Houlsby. An image is worth 16x16 words: Transformers for image recognition at scale. In *International Conference on Learning Representations*, 2021. 5, 4
- [10] Yu Du, Fangyun Wei, Ziheng Zhang, Miaojing Shi, Yue Gao, and Guoqi Li. Learning to prompt for open-vocabulary object detection with vision-language model. In *Proceedings of the IEEE/CVF Conference on Computer Vision and Pattern Recognition*, pages 14084–14093, 2022. 1
- [11] Li Fei-Fei, Rob Fergus, and Pietro Perona. Learning generative visual models from few training examples: An incremental bayesian approach tested on 101 object categories. In *2004 conference on computer vision and pattern recognition workshop*, pages 178–178. IEEE, 2004. 5
- [12] Chengjian Feng, Yujie Zhong, Zequn Jie, Xiangxiang Chu, Haibing Ren, Xiaolin Wei, Weidi Xie, and Lin Ma. Prompt-det: Towards open-vocabulary detection using uncurated images. In *European Conference on Computer Vision*, pages 701–717. Springer, 2022. 1
- [13] Dominik Fuchsruber, Tom Wollschläger, Bertrand Chappentier, Antonio Oroz, and Stephan Günnemann. Uncertainty for active learning on graphs. In *Forty-first International Conference on Machine Learning*, 2024. 3
- [14] Golnaz Ghiasi, Xiuye Gu, Yin Cui, and Tsung-Yi Lin. Scaling open-vocabulary image segmentation with image-level labels. In *European Conference on Computer Vision*, pages 540–557. Springer, 2022. 1
- [15] Sanket Rajan Gupte, Josiah Aklilu, Jeffrey J Nirschl, and Serena Yeung-Levy. Revisiting active learning in the era of vision foundation models. *Transactions on Machine Learning Research*, 2024. 3
- [16] Guy Hacohen and Daphna Weinshall. How to select which active learning strategy is best suited for your specific problem and budget. In *Advances in Neural Information Processing Systems*, pages 13395–13407. Curran Associates, Inc., 2023. 3
- [17] Guy Hacohen and Daphna Weinshall. How to select which active learning strategy is best suited for your specific problem and budget. In *Thirty-seventh Conference on Neural Information Processing Systems*, 2023.
- [18] Guy Hacohen, Avihu Dekel, and Daphna Weinshall. Active learning on a budget: Opposite strategies suit high and low budgets. In *International Conference on Machine Learning*, pages 8175–8195. PMLR, 2022. 3
- [19] Tao He, Xiaoming Jin, Guiguang Ding, Lan Yi, and Chenggang Yan. Towards better uncertainty sampling: Active learning with multiple views for deep convolutional neural network. In *IEEE International Conference on Multimedia and Expo (ICME)*, 2019. 3
- [20] Patrick Helber, Benjamin Bischke, Andreas Dengel, and Damian Borth. Eurosat: A novel dataset and deep learning benchmark for land use and land cover classification. *IEEE Journal of Selected Topics in Applied Earth Observations and Remote Sensing*, 12(7):2217–2226, 2019. 8
- [21] Alex Holub, Pietro Perona, and Michael C Burl. Entropy-based active learning for object recognition. In *2008 IEEE Computer Society Conference on Computer Vision and Pattern Recognition Workshops*, pages 1–8. IEEE, 2008. 5
- [22] Sehyun Hwang, Sohyun Lee, Sungyeon Kim, Jungseul Ok, and Suha Kwak. Combating label distribution shift for active domain adaptation. In *ECCV*, pages 549–566. Springer, 2022. 3
- [23] Sehyun Hwang, Sohyun Lee, Hoyoung Kim, Minhyeon Oh, Jungseul Ok, and Suha Kwak. Active learning for semantic segmentation with multi-class label query. In *Advances in Neural Information Processing Systems*, pages 27020–27039. Curran Associates, Inc., 2023. 3
- [24] Chao Jia, Yinfei Yang, Ye Xia, Yi-Ting Chen, Zarana Parekh, Hieu Pham, Quoc Le, Yun-Hsuan Sung, Zhen Li, and Tom

- Duerig. Scaling up visual and vision-language representation learning with noisy text supervision. In *International conference on machine learning*, pages 4904–4916. PMLR, 2021. 1
- [25] Muhammad Uzair Khattak, Hanoona Rasheed, Muhammad Maaz, Salman Khan, and Fahad Shahbaz Khan. Maple: Multi-modal prompt learning. In *Proceedings of the IEEE/CVF Conference on Computer Vision and Pattern Recognition*, pages 19113–19122, 2023. 1, 2, 7
- [26] Muhammad Uzair Khattak, Syed Talal Wasim, Muzammal Naseer, Salman Khan, Ming-Hsuan Yang, and Fahad Shahbaz Khan. Self-regulating prompts: Foundational model adaptation without forgetting. In *Proceedings of the IEEE/CVF International Conference on Computer Vision*, pages 15190–15200, 2023. 2, 7
- [27] Hoyoung Kim, Minhyeon Oh, Sehyun Hwang, Suha Kwak, and Jungseul Ok. Adaptive superpixel for active learning in semantic segmentation. In *Proceedings of the IEEE/CVF International Conference on Computer Vision (ICCV)*, pages 943–953, 2023. 3
- [28] Hoyoung Kim, Sehyun Hwang, Suha Kwak, and Jungseul Ok. Active label correction for semantic segmentation with foundation models. In *Forty-first International Conference on Machine Learning*, 2024. 3
- [29] Alexander Kirillov, Eric Mintun, Nikhila Ravi, Hanzi Mao, Chloe Rolland, Laura Gustafson, Tete Xiao, Spencer Whitehead, Alexander C Berg, Wan-Yen Lo, et al. Segment anything. In *Proceedings of the IEEE/CVF International Conference on Computer Vision*, pages 4015–4026, 2023. 2
- [30] Jonathan Krause, Michael Stark, Jia Deng, and Li Fei-Fei. 3d object representations for fine-grained categorization. In *Proceedings of the IEEE international conference on computer vision workshops*, pages 554–561, 2013. 5
- [31] Boyi Li, Kilian Q Weinberger, Serge Belongie, Vladlen Koltun, and Rene Ranftl. Language-driven semantic segmentation. In *International Conference on Learning Representations*, 2022. 1
- [32] Juncheng Li, Minghe Gao, Longhui Wei, Siliang Tang, Wenqiao Zhang, Mengze Li, Wei Ji, Qi Tian, Tat-Seng Chua, and Yueting Zhuang. Gradient-regulated meta-prompt learning for generalizable vision-language models. In *Proceedings of the IEEE/CVF International Conference on Computer Vision*, pages 2551–2562, 2023. 2
- [33] Yunfan Li, Peng Hu, Dezhong Peng, Jiancheng Lv, Jianping Fan, and Xi Peng. Image clustering with external guidance. In *Forty-first International Conference on Machine Learning*, 2024. 2
- [34] James MacQueen et al. Some methods for classification and analysis of multivariate observations. In *Proceedings of the fifth Berkeley symposium on mathematical statistics and probability*, pages 281–297. Oakland, CA, USA, 1967. 1, 4
- [35] Rafid Mahmood, Sanja Fidler, and Marc T Law. Low-budget active learning via wasserstein distance: An integer programming approach. In *International Conference on Learning Representations*, 2021. 1
- [36] Subhransu Maji, Esa Rahtu, Juho Kannala, Matthew Blaschko, and Andrea Vedaldi. Fine-grained visual classification of aircraft. *arXiv preprint arXiv:1306.5151*, 2013. 5
- [37] Maria-Elena Nilsback and Andrew Zisserman. Automated flower classification over a large number of classes. In *2008 Sixth Indian conference on computer vision, graphics & image processing*, pages 722–729. IEEE, 2008. 5
- [38] OpenAI. Gpt-4 technical report. *arXiv preprint arXiv:2303.08774*, 2023. 2
- [39] Natalia Ostapuk, Jie Yang, and Philippe Cudré-Mauroux. Activelink: deep active learning for link prediction in knowledge graphs. In *The World Wide Web Conference (WWW)*, 2019. 3
- [40] Jinyoung Park, Juyeon Ko, and Hyunwoo J Kim. Prompt learning via meta-regularization. In *Proceedings of the IEEE/CVF Conference on Computer Vision and Pattern Recognition*, pages 26940–26950, 2024. 1, 2, 7
- [41] Omkar M Parkhi, Andrea Vedaldi, Andrew Zisserman, and CV Jawahar. Cats and dogs. In *2012 IEEE conference on computer vision and pattern recognition*, pages 3498–3505. IEEE, 2012. 5
- [42] Alec Radford, Jong Wook Kim, Chris Hallacy, Aditya Ramesh, Gabriel Goh, Sandhini Agarwal, Girish Sastry, Amanda Askell, Pamela Mishkin, Jack Clark, et al. Learning transferable visual models from natural language supervision. In *International conference on machine learning*, pages 8748–8763. PMLR, 2021. 1, 2, 3, 5, 4
- [43] Shiori Sagawa, Pang Wei Koh, Tatsunori B Hashimoto, and Percy Liang. Distributionally robust neural networks. In *International Conference on Learning Representations*. 7
- [44] Ramprasaath R Selvaraju, Michael Cogswell, Abhishek Das, Ramakrishna Vedantam, Devi Parikh, and Dhruv Batra. Grad-cam: Visual explanations from deep networks via gradient-based localization. In *Proceedings of the IEEE international conference on computer vision*, pages 618–626, 2017. 2, 4, 1
- [45] Ozan Sener and Silvio Savarese. Active learning for convolutional neural networks: A core-set approach. In *International Conference on Learning Representations*, 2018. 3, 5
- [46] Amanpreet Singh, Ronghang Hu, Vedanuj Goswami, Guillaume Couairon, Wojciech Galuba, Marcus Rohrbach, and Douwe Kiela. Flava: A foundational language and vision alignment model. In *Proceedings of the IEEE/CVF Conference on Computer Vision and Pattern Recognition*, pages 15638–15650, 2022. 1
- [47] Samarth Sinha, Sayna Ebrahimi, and Trevor Darrell. Variational adversarial active learning. In *ICCV*, 2019. 3
- [48] K Soomro. Ucf101: A dataset of 101 human actions classes from videos in the wild. *arXiv preprint arXiv:1212.0402*, 2012. 5
- [49] Laurens Van der Maaten and Geoffrey Hinton. Visualizing data using t-sne. *Journal of machine learning research*, 9 (11), 2008. 2, 7
- [50] Tianjiao Wan, Kele Xu, Ting Yu, Xu Wang, Dawei Feng, Bo Ding, and Huaimin Wang. A survey of deep active learning for foundation models. *Intelligent Computing*, 2:0058, 2023. 3

- [51] Zengmao Wang, Bo Du, Weiping Tu, Lefei Zhang, and Dacheng Tao. Incorporating distribution matching into uncertainty for multiple kernel active learning. *IEEE Transactions on Knowledge and Data Engineering (TKDE)*, 2019. [3](#)
- [52] Jianxiong Xiao, James Hays, Krista A Ehinger, Aude Oliva, and Antonio Torralba. Sun database: Large-scale scene recognition from abbey to zoo. In *2010 IEEE computer society conference on computer vision and pattern recognition*, pages 3485–3492. IEEE, 2010. [5](#)
- [53] Ofer Yehuda, Avihu Dekel, Guy Hacohen, and Daphna Weinshall. Active learning through a covering lens. *Advances in Neural Information Processing Systems*, 35: 22354–22367, 2022. [3](#)
- [54] Muyang Yi, Quan Cui, Hao Wu, Cheng Yang, Osamu Yoshie, and Hongtao Lu. A simple framework for text-supervised semantic segmentation. In *Proceedings of the IEEE/CVF Conference on Computer Vision and Pattern Recognition*, pages 7071–7080, 2023. [1](#)
- [55] Lu Yuan, Dongdong Chen, Yi-Ling Chen, Noel Codella, Xiyang Dai, Jianfeng Gao, Houdong Hu, Xuedong Huang, Boxin Li, Chunyuan Li, et al. Florence: A new foundation model for computer vision. *arXiv preprint arXiv:2111.11432*, 2021. [1](#)
- [56] Xiaohua Zhai, Xiao Wang, Basil Mustafa, Andreas Steiner, Daniel Keysers, Alexander Kolesnikov, and Lucas Beyer. Lit: Zero-shot transfer with locked-image text tuning. In *Proceedings of the IEEE/CVF conference on computer vision and pattern recognition*, pages 18123–18133, 2022. [1](#)
- [57] Yiwu Zhong, Jianwei Yang, Pengchuan Zhang, Chunyuan Li, Noel Codella, Liunian Harold Li, Luwei Zhou, Xiyang Dai, Lu Yuan, Yin Li, et al. Regionclip: Region-based language-image pretraining. In *Proceedings of the IEEE/CVF conference on computer vision and pattern recognition*, pages 16793–16803, 2022. [1](#)
- [58] Kaiyang Zhou, Jingkang Yang, Chen Change Loy, and Ziwei Liu. Conditional prompt learning for vision-language models. In *Proceedings of the IEEE/CVF conference on computer vision and pattern recognition*, pages 16816–16825, 2022. [1](#), [2](#)
- [59] Kaiyang Zhou, Jingkang Yang, Chen Change Loy, and Ziwei Liu. Learning to prompt for vision-language models. *International Journal of Computer Vision*, 130(9):2337–2348, 2022. [1](#), [2](#), [3](#), [5](#), [8](#), [4](#)
- [60] Beier Zhu, Yulei Niu, Yucheng Han, Yue Wu, and Hanwang Zhang. Prompt-aligned gradient for prompt tuning. In *Proceedings of the IEEE/CVF International Conference on Computer Vision*, pages 15659–15669, 2023. [1](#), [2](#)

# Active Prompt Learning with Vision-Language Model Priors

## Supplementary Material

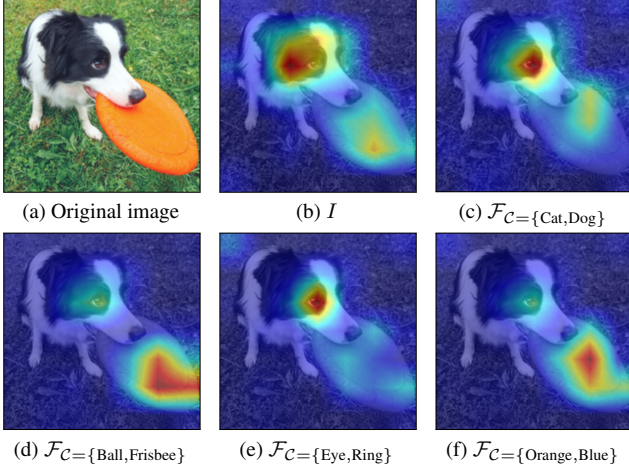


Figure 7. *GradFAM with various target features.* (b) All objects in the image have a significant impact on the target image features  $I$ . (c-f) Using our class-guided features  $\mathcal{F}_C$  for the target features, the heatmap closely aligns with the target classes  $\mathcal{C}$ .

### A. Details of GradFAM

In Section 4.1, we propose class-guided features and analyze them with our GradFAM, a modified version of Grad-CAM [44]. Here, we provide a detailed description of GradFAM and its differences from GradCAM.

**Gradient-Weighted Class Activation Map (CAM).** To highlight the importance of regions in an image  $x$  associated with a given class  $c$ , Grad-CAM introduces the class-discriminative localization map as follows:

$$L_{\text{CAM}}^c(x) \in \mathbb{R}^{U \times V}, \quad (14)$$

where  $U$  and  $V$  are the width and height of the image  $x$ .

Let  $f(x; \theta) \in \mathbb{R}^{|\mathcal{C}|}$  represent the output logits of a neural network with parameters  $\theta$ , where  $|\mathcal{C}|$  is the total number of classes. For a given class  $c \in \mathcal{C}$ , the score  $y^c(x; \theta)$  is defined as follows:

$$y^c(x; \theta) := f_c(x; \theta), \quad (15)$$

where  $f_c(x; \theta)$  denotes the  $c$ -th logit value, representing the model’s confidence for class  $c$  given the image  $x$ . Grad-CAM computes the gradient of  $y^c(x; \theta)$  with respect to the activation maps  $A^k$  in the last convolutional layer, where  $A^k \in \mathbb{R}^{W \times H}$  represents the activation map of the  $k$ -th channel with spatial dimensions  $W$  and  $H$ . Note that  $W$  and  $H$  are typically smaller than  $U$  and  $V$  due to downsampling in the convolutional layers.

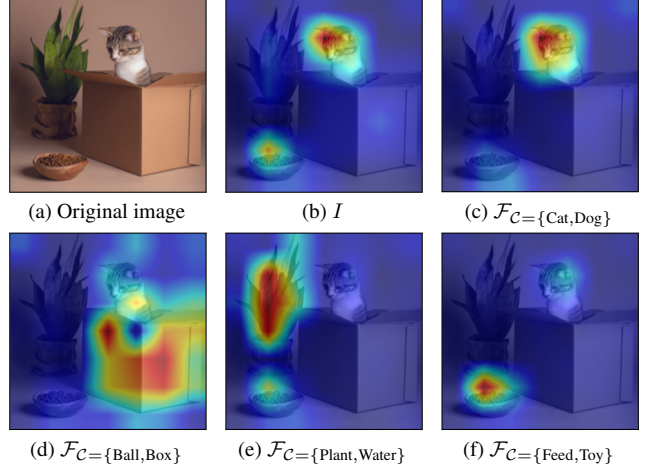


Figure 8. *GradFAM with various target features.* (b) All objects in the image have a significant impact on the target image features  $I$ . (c-f) Using our class-guided features  $\mathcal{F}_C$  for the target features, the heatmap closely aligns with the target classes  $\mathcal{C}$ .

The importance weight  $\alpha_c^k$  for each channel  $k$  is obtained by applying global average pooling over the gradients as:

$$\alpha_{\text{CAM}}^{c,k} := \frac{1}{W \times H} \sum_{w=1}^W \sum_{h=1}^H \frac{\partial y^c(x; \theta)}{\partial A_{w,h}^k}, \quad (16)$$

representing the overall importance of the  $k$ -th feature map for predicting class  $c$ .

The class-discriminative localization map  $L_{\text{CAM}}^c(x)$  is then computed as a weighted combination of the activation maps, followed by upsampling to match the dimensions of the input image  $x$ :

$$L_{\text{CAM}}^c(x) := \mathcal{U} \left( \text{ReLU} \left( \sum_k \alpha_{\text{CAM}}^{c,k} A^k \right) \right), \quad (17)$$

where  $\mathcal{U}$  denotes the upsampling function.

**Gradient-Weighted Feature Activation Map (FAM).** To adapt GradCAM for vision-language models (VLMs), such as CLIP, which consist of an image encoder  $\theta_{\text{img}}$  and a text encoder  $\theta_{\text{txt}}$ , we redefine the weight  $\alpha$  with target features  $\mathcal{F}_{\text{target}}$  as follows:

$$\alpha_{\text{FAM}}^k := \frac{1}{W \times H} \sum_{w=1}^W \sum_{h=1}^H \frac{\partial \cos(\theta_{\text{img}}(x), \mathcal{F}_{\text{target}})}{\partial A_{w,h}^k}, \quad (18)$$

representing the overall important of the  $k$ -th feature map in determining the cosine similarity between the image features  $\theta_{\text{img}}(x)$  and the target features  $\mathcal{F}_{\text{target}}$ . Here, the key



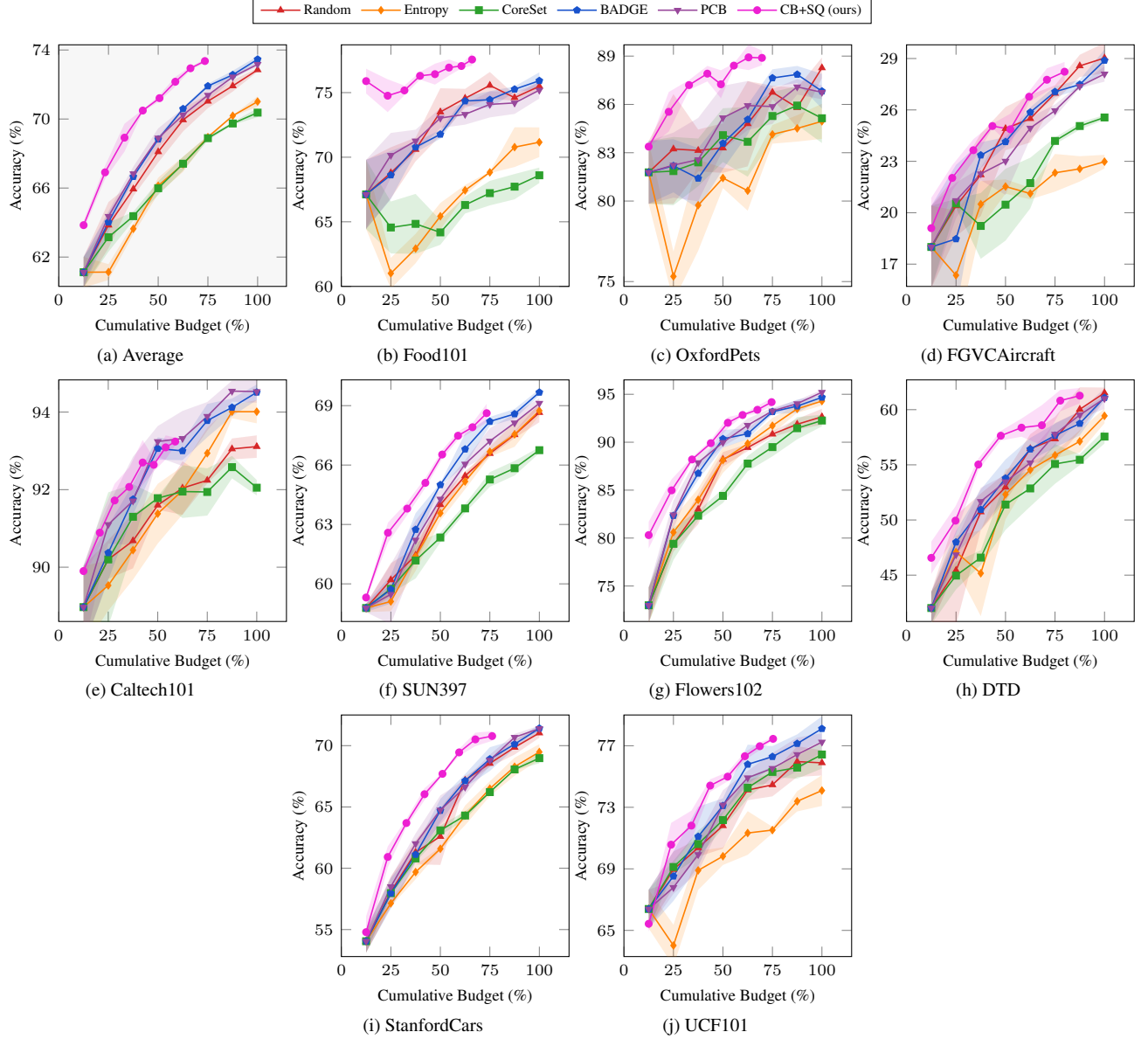


Figure 9. *Effect of the proposed acquisition.* (a) Our CB+SQ outperforms the other baselines in average performance across 9 datasets. (b-j) We achieve comparable performance to other baselines, while reducing the labeling budget by 12% to 41% across all datasets.

difference from the GradCAM’s weights in (16) lies in the absence of a specific class  $c$ . This modification enables the use of GradFAM for more flexible and label-independent analyses, accommodating the multimodal nature of VLMs. Building on this, the target feature discriminative localization map  $L_{\text{FAM}}(x)$  is then computed as:

$$L_{\text{FAM}}(x) := \mathcal{U} \left( \text{ReLU} \left( \sum_k \alpha_{\text{FAM}}^k A^k \right) \right). \quad (19)$$

Our GradFAM can visualize the importance of various target features on the image, including (i)  $\mathcal{F}_{\text{target}} = \theta_{\text{txt}}(c)$ ,

(ii)  $\mathcal{F}_{\text{target}} = \theta_{\text{img}}(x)$ , and (iii)  $\mathcal{F}_{\text{target}} = \mathcal{F}_C(x)$ . Specifically, when  $\mathcal{F}_{\text{target}} = \theta_{\text{txt}}(c)$ , our GradFAM operates almost identically to the original GradCAM. For  $\mathcal{F}_{\text{target}} = \theta_{\text{img}}(x)$ , due to VLMs being trained through contrastive learning to align images and texts in a shared embedding space, all objects in the image are highlighted, as shown in Figures 7b and 8b. In the case of our class-guided features  $\mathcal{F}_C(x)$  in (7), the guiding class set  $\mathcal{C}$  effectively highlights the corresponding objects, as illustrated in Figures 7 and 8.

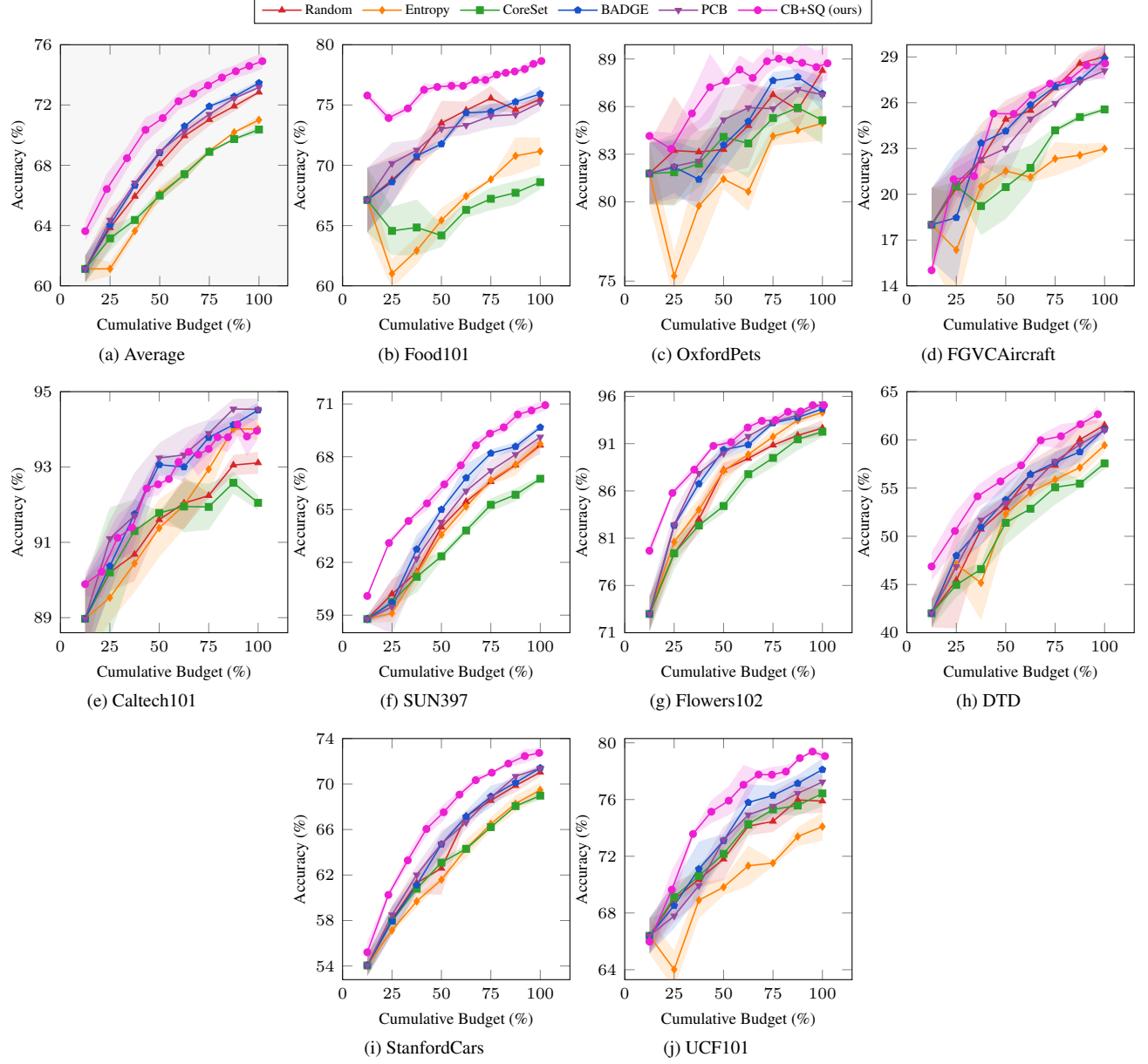


Figure 10. *Effect of proposed acquisition with the same budget.* (a) Our CB+SQ outperforms the other baselines in average performance across 9 datasets.

Method	Food101	OxfordPets	Aircraft	Caltech101	SUN397	Flowers102	DTD	StanfordCars	UCF101	Average (%)
MaPle	74.47	86.80	21.87	92.53	64.67	83.73	52.23	61.97	71.67	67.77
+ CB	75.97	87.00	<b>21.93</b>	92.03	64.67	<b>86.10</b>	52.67	62.17	71.63	68.24
+ CB*	<b>78.60</b>	<b>87.10</b>	21.80	<b>93.50</b>	<b>66.10</b>	85.83	<b>54.43</b>	<b>63.70</b>	<b>75.17</b>	<b>69.58</b>
PromptSRC	79.63	89.83	24.97	94.27	69.17	85.00	55.87	66.00	75.03	71.09
+ CB	80.77	89.90	24.63	93.63	69.23	86.10	57.40	64.97	74.27	71.21
+ CB*	<b>81.40</b>	<b>90.47</b>	<b>26.13</b>	<b>94.47</b>	<b>70.17</b>	<b>87.07</b>	<b>59.03</b>	<b>66.27</b>	<b>76.97</b>	<b>72.44</b>
ProMetaR	78.50	89.13	22.70	93.43	67.5	86.47	55.5	64.7	74.03	70.22
+ CB	79.67	89.27	23.23	93.27	67.97	88.10	57.27	64.67	73.83	70.81
+ CB*	<b>80.53</b>	<b>89.63</b>	<b>24.23</b>	<b>94.23</b>	<b>69.20</b>	<b>88.47</b>	<b>58.93</b>	<b>66.20</b>	<b>77.17</b>	<b>72.07</b>

Table 5. *Synergy of the proposed acquisition with existing prompt learning methods.* The model-centric prompt learning methods utilize the improved datasets denoted as CB and CB\*, achieving higher classification performance compared to conventional few-shot datasets.

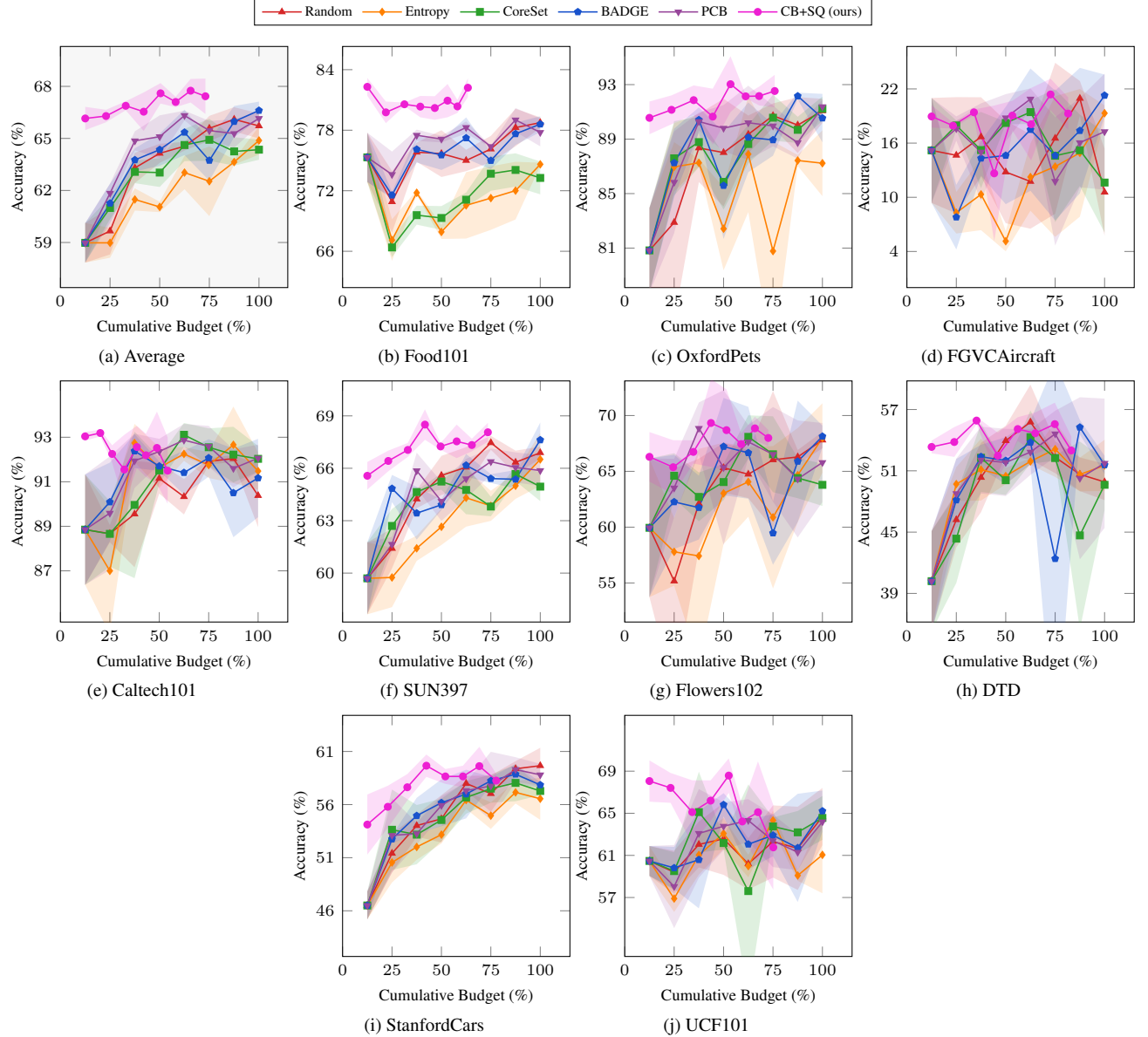


Figure 11. *Harmonic mean accuracy*. (a) Our CB+SQ outperforms the other baselines in average performance across 9 datasets. (b-j) The fluctuation in harmonic mean performance is attributed to variations in performance on novel classes, stemming from the limitations of the base prompt learning method, CoOp [59].

## B. Additional Experiments

In Section 5, we perform extensive experiments across various situations. In this section, we provide additional experimental results omitted from the main paper.

**Implementation Details.** In our experiments, we employ CLIP ViT-B/32 [9, 42] as our VLM. At each round  $r$ , we reinitialize the learnable prompts  $t_r$ , consisting of 16 vectors, using a Gaussian distribution with a mean of 0 and a standard deviation of 0.02. Following the training details in CoOp [59], we train these prompts for 200 epochs per round

using the SGD optimizer, initialized with a learning rate of 0.002 and decaying according to a cosine annealing.

**Active Learning with Fixed Rounds.** In Figure 9, we report the results for all datasets using the same experimental setup as in Figure 3. Figure 9 demonstrates that our method CB+SQ outperforms other baselines across datasets.

**Active Learning with Fixed Budgets.** For fair comparisons, we evaluate our CB+SQ alongside with baselines over eight rounds, as illustrated in Figures 3 and 9. How-

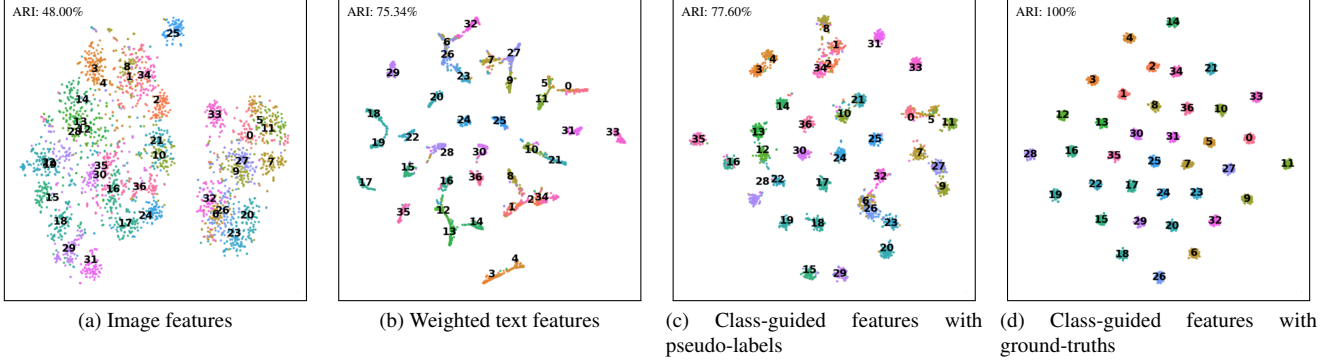


Figure 12. *Various clustering methods on OxfordPets dataset.* (a) Clustering based solely on image features primarily separates the data into two large groups, corresponding to dogs and cats, but fails to capture finer details. (b) Clustering on weighted text features improves Adjusted Rand Index (ARI), but some clusters remain ambiguous. (c) Class-guided clustering with pseudo-labels produces more distinct clusters, aligned with the guided class set  $|\mathcal{C}| = 37$ . (d) Class-guided clustering with ground truth shows perfect alignment of clusters.

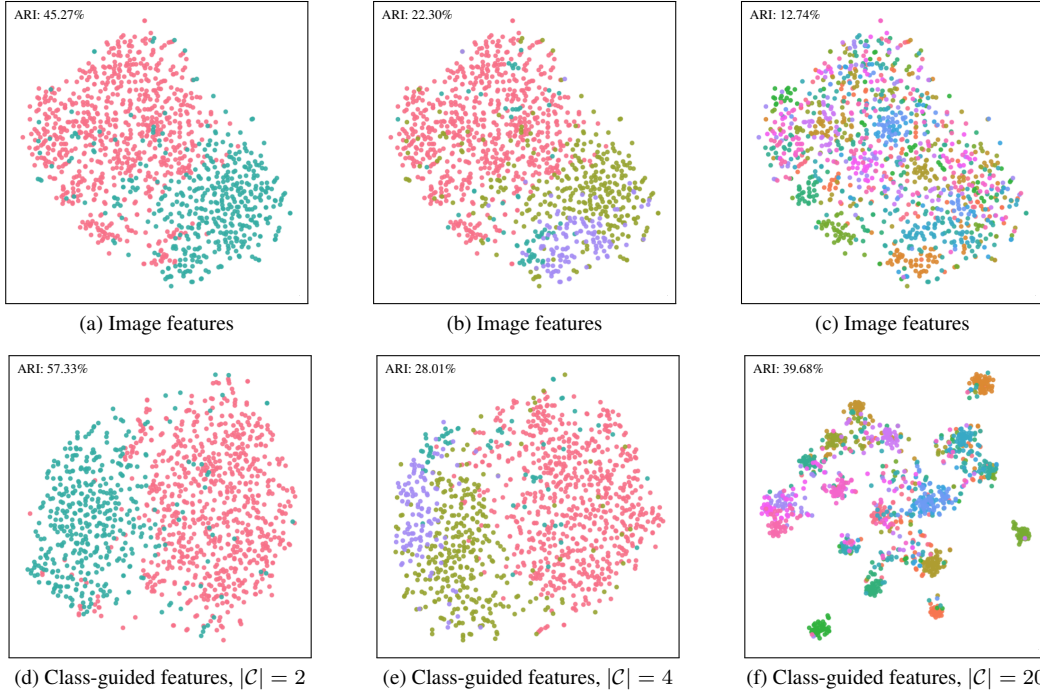


Figure 13. *Class-guided clustering on WaterBirds dataset* (a, b, c) Clustering based solely on image features results in clusters that are poorly separated. (d, e, f) In contrast, our class-guided clustering, which incorporates class information, leads to more distinct clusters that align with the size of the guiding class set  $\mathcal{C}$ .

ever, thanks to our selective querying in Section 4.3, we conserve budgets for each round. Here, we conduct additional experiments using the same budget. Figure 10 shows that our CB+SQ outperforms the baselines under various budget scenarios.

**Extensions to SOTA Model-Centric Prompt Learning Methods.** In Table 1, we integrate our CB acquisition function with SOTA model-centric prompt learning methods,

utilizing given 1-shot labeled datasets, where each class contains a single image, *i.e.*  $B = |\mathcal{C}|$ . In Table 5, we extend our experiments to 2-shot labeled datasets, where each class contains two images, *i.e.*  $B = 2 \times |\mathcal{C}|$ . Our CB and CB\*-based datasets consistently outperform conventional few-shot labeled datasets across nine datasets. Importantly, our data-centric approach is compatible with existing model-centric approaches, offering further efficiency in adapting VLMs to new tasks.



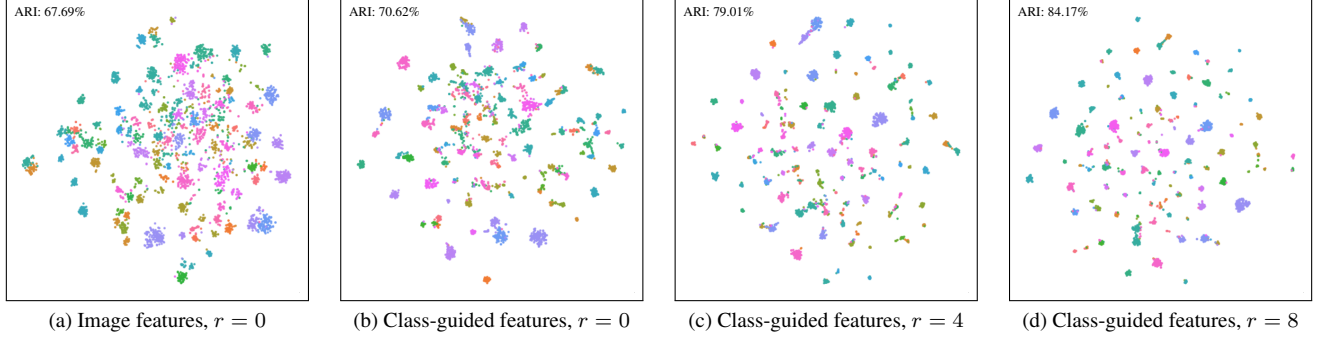


Figure 14. *Class-guided clustering across different rounds.* (a, b) In the initial round, *i.e.*  $r = 0$ , clustering on class-guided features achieves a higher ARI compared to clustering on image features. (c, d) We observe an improvement in ARI performance as the rounds progress.

Index	Name	Index	Name	Index	Name	Index	Name
019	Gray Catbird	027	Shiny Cowbird	029	American Crow	032	Mangrove Cuckoo
046	Gadwall	057	Rose-breasted Grosbeak	058	Pigeon Guillemot	061	Heermann’s Gull
069	Rufous Hummingbird	073	Blue Jay	079	Belted Kingfisher	098	Scott Oriole
116	Chipping Sparrow	121	Grasshopper Sparrow	125	Lincoln Sparrow	155	Warbling Vireo
167	Hooded Warbler	172	Nashville Warbler	174	Palm Warbler	185	Bohemian Waxwing

Table 6. *Examples of guiding class set.* To improve the clarity of clustering visualization, we randomly subsample 20 classes from the total of 200 classes.

$ \mathcal{C} $	$\mathcal{C}$
2	land background water background
4	land bird on land background land bird on water background water bird on land background water bird on water background

Table 7. *Various guiding class sets.* Based on two habitats and two backgrounds, we construct class sets comprising 2 and 4 classes.

**Base-to-Novel Generalization.** In Table 4, our CB acquisition achieves superior harmonic mean accuracy compared to Random in the initial round. Here, we further extend our experiments across eight rounds. After the initial round, our method transitions to CB+SQ, as selective querying becomes applicable from the second round onward. Figure 11 illustrates the higher generalization capabilities of our CB+SQ compared to other baselines. Specifically, the benefit of our method is pronounced in the initial round.

### C. Analyses of Class-Guided Clustering

In Figure 4, we visualize the difference between class-guided clustering and conventional clustering based on image features. In this section, we present additional analyses on various clustering methods across different datasets and rounds.

**Class-Guided Clustering on OxfordPets Dataset.** In Figure 12, we analyze various clustering methods, including clustering on image features in (5), (b) weighted text features in (6), (c) class-guided features with pseudo-labels in (7), (d) class-guided features with ground-truth labels, where the weights of weighted text features are replaced to ground-truth labels, *i.e.* one-hot encodings on labels. Figure 12 illustrates that clustering on class-guided features achieves higher Adjusted Rand Index (ARI) values. Especially, Figure 12d suggests that as the performance of VLMs improves, perfect clustering becomes achievable.

**Class-Guided Clustering on WaterBirds Dataset.** In Section 5.3 and Figure 4, we introduce the WaterBirds dataset to demonstrate the benefits of class-guided clustering, where different classes are guided within the same dataset. Specifically, the Waterbirds dataset comprises 200 distinct bird species, with each image annotated by habitat (water, land), background (water, land), and specific species. For our analyses, we select 20 classes and leverage various label information to separate the subset into groups of 2, 4, and 20 classes. Tables 6 and 7 provide the detailed class names. We note that text prompts such as “a photo of a ” are prepended to each class  $c \in \mathcal{C}$  to generate final prompts. As shown in Figure 13, class-guided features based on different sizes of guiding class sets  $\mathcal{C}$  effectively represent class-specific information.

Method	Food101	OxfordPets	Aircraft	Caltech101	SUN397	Flowers102	DTD	StanfordCars	UCF101	Avg. (%)
Euclidean Dist.	76.16	84.18	19.10	<b>89.41</b>	59.46	79.02	46.47	<b>55.32</b>	65.21	63.82
Cosine Sim.	<b>77.18</b>	<b>87.58</b>	<b>20.05</b>	89.37	<b>60.37</b>	<b>79.63</b>	<b>47.26</b>	54.70	63.59	<b>64.42</b>

Table 8. *Various distance metrics for K-means clustering.* K-means clustering based on cosine similarity shows greater effectiveness compared to Euclidean distance.

Methods	Round 1	Round 2	Round 3	Round 4	Round 5	Round 6	Round 7	Round 8
$K = B$	63.65 $\pm$ 0.16	66.37 $\pm$ 0.16	67.07 $\pm$ 0.49	68.34 $\pm$ 0.46	69.15 $\pm$ 0.16	69.43 $\pm$ 0.36	69.96 $\pm$ 0.10	70.28 $\pm$ 0.21
$K = 8 \times B$	59.77 $\pm$ 0.27	64.30 $\pm$ 0.59	67.33 $\pm$ 0.57	69.30 $\pm$ 0.48	70.62 $\pm$ 0.63	71.92 $\pm$ 0.54	72.46 $\pm$ 0.32	72.96 $\pm$ 0.26
$K = r \times B$	<b>63.85</b> $\pm$ 0.26	<b>66.91</b> $\pm$ 0.38	<b>68.92</b> $\pm$ 0.81	<b>70.49</b> $\pm$ 0.06	<b>71.21</b> $\pm$ 0.18	<b>72.16</b> $\pm$ 0.28	<b>72.94</b> $\pm$ 0.09	<b>73.34</b> $\pm$ 0.12

Table 9. *Various values of K for K-means clustering.* Our progressively increasing K across rounds achieves the best performance throughout all rounds.

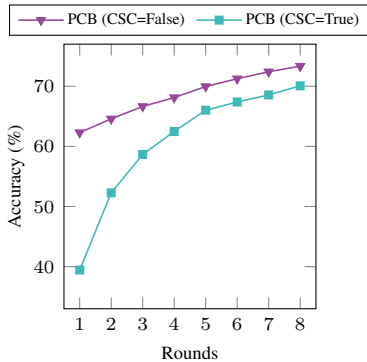


Figure 15. *Ablation on PCB.* When class-specific context (CSC) is set to False, *i.e.* unified prompts across all classes, PCB demonstrates improved performance.

**Cluster-Guided Clustering with Various Rounds.** We analyze the impact of class-guided clustering, derived from the zero-shot CLIP model, in comparison to various other clustering methods before initiating active learning. Here, we investigate cluster-guided clustering on the OxfordFlowers dataset, utilizing text prompts that evolve with each round. Figure 14 illustrates that as the rounds progress, class-guided clustering forms increasingly well-separated clusters, accompanied by a steady increase in ARI.

## D. Ablation on K-means Clustering

**Euclidean Distance vs. Cosine Similarity.** Our algorithm employs K-means clustering, as outlined in Algorithm 1, with K centroids updated based on Euclidean distance. However, since CLIP performs inference using cosine similarity, we also explore updating the centroids with cosine similarity. Table 8 demonstrates that cosine similarity-based K-means clustering improves overall performance, especially on specific datasets like OxfordPets. Nonetheless, we use Euclidean distance for all other experiments,

except for the results shown in Table 8.

**Effect of Various K.** In Section 4.2, we set K equal to the budget B in the initial round and introduce a linearly increasing K according to round r, *i.e.*  $K = r \times B$ . Here, we analyze the effect of this increasing K. Table 9 shows that fixed values of K, whether small ( $K = B$ ) or large ( $K = 8 \times B$ ), are less effective compared to our incrementally increasing K. Specifically, using a small K results in multiple samples being selected from the same cluster, leading to redundancy and reduced performance. On the other hand, a large K fails to select representative samples during the initial round, resulting in diminished performance.

## E. Ablation on PCB

The recent state-of-the-art active prompt learning method for VLMs, called PCB [4], employs class-specific prompts, with each class assigned a distinct prompt. In contrast, our experiments adopt unified prompts, where all classes share the same prompt. This choice, as illustrated in Figure 15, demonstrates the substantial benefits of using unified prompts, *i.e.* with class-specific context (CSC) set to False.